Alteration of the pH Dependence of Coronavirus-Induced Cell Fusion: Effect of Mutations in the Spike Glycoprotein†

THOMAS M. GALLAGHER,* CRISTINA ESCARMIS,‡ AND MICHAEL J. BUCHMEIER

Department of Neuropharmacology, Scripps Clinic and Research Foundation, La Jolla, California 92037

Infection of susceptible murine cells with the coronavirus mouse hepatitis virus type 4 (MHV4) results in extensive cell-cell fusion at pHs from 5.5 to 8.5. The endosomotropic weak bases chloroquine and ammonium chloride do not prevent MHV4 infection. In marked contrast, we have selected variants from a neural cell line persistently infected with MHV4 which are entirely dependent on acid pH to fuse host cells and are strongly inhibited by endosomotropic weak bases. Wild-type and variant viruses were compared at the level of the fusion-active surface (S) glycoprotein gene. Cloning and sequencing of each 4,131-base open reading frame predicted a total of eight amino acid differences which fell into three distinct clusters. Each S glycoprotein, when expressed from cDNA, was synthesized in equivalent amounts, and similar proportions were transported to the cell surface. Wild-type S induced cell-cell fusion at neutral pH, whereas variant S required prolonged exposure to acidic pH to induce fusion. Expression of hybrid S genes prepared by exchange of restriction fragments between wild-type and variant cDNAs revealed that elimination of neutral pH fusion was solely dependent on amino acid alterations at positions 1067 (Q to H), 1094 (Q to H), and 1114 (L to R). These changes lie within a predicted heptad repeat region of the transmembrane cleavage fragment of S (S2). These findings demonstrate that the pH dependence of coronavirus fusion is highly variable and that this variability can be determined by as few as three amino acid residues.

Delivery of the internal nucleocapsid of enveloped viruses into the host cell requires virus binding to cellular receptors followed by fusion of viral and cellular membranes. Both of these events are mediated by viral surface glycoproteins. For coronaviruses, these functions are provided by a single glycoprotein termed S (for spike or surface) (3, 33, 42). Following receptor binding, S mediates a pH-independent fusion reaction (12, 38, 42) which initiates the delivery of infectious virion RNA to host cytosol. This fusion reaction is also readily evident late in the infection cycle, when S expression at the cell surface results in fusion of plasma membranes and formation of multinucleated syncytia. Thus, S-mediated coronavirus fusion differs from the acid pH-dependent fusion found among a variety of other enveloped RNA viruses, including orthomyxo-, toga-, and rhabdoviruses (45). Acid pH-dependent fusion occurs only after internalization of virus in acidic endosomes, where protonation of critical residues on a viral envelope glycoprotein alters its conformation and exposes a hydrophobic "fusion peptide" domain (34). Viruses that require acid exposure to activate fusion generate multinucleated syncytia only after deliberate reduction of extracellular pH.

The coronavirus S glycoprotein is a 180- to 200-kDa molecule that is cotranslationally glycosylated in the endoplasmic reticulum (24). Most of the S population is then oligomerized into a trimeric structure (4, 8). These S oligomers are transported toward the Golgi, where a large portion become incorporated into virions budding into pre-Golgi vesicles (41, 42). S glycoproteins then continue through the exocytic pathway, after which in most cases they undergo proteolytic cleavage into two similar-sized fragments, an amino-terminal S1 and a carboxy-terminal S2 (38). Virions are released into the extracellular medium, whereas free S glycoprotein is expressed at the cell surface and induces fusion with neighboring cell membranes.

Primary structures determined from the nucleotide sequences of a number of coronavirus S genes (33) have revealed several common structural features. All S glycoproteins possess hydrophobic domains located at the termini of the linear amino acid sequence. The amino-terminal apolar residues have properties characteristic of a signal sequence (43), while the carboxy-terminal hydrophobicity serves as a transmembrane domain anchoring the S2 fragment (4, 39). No other linear stretches of hydrophobic residues are present. Thus, the S glycoprotein is unlike those found on viruses belonging to a variety of other families in that it lacks a third hydrophobic fusion peptide domain (18, 45).

A second shared structural feature in coronavirus S glycoproteins is an extensive heptad repeat region within the S2 posttranslational cleavage fragment (7). A heptad repeat is characterized by a sequence periodicity of the form (a-b-c-d-e-f-g)$_n$, in which the residues at positions a and d are apolar (5). Such a motif in S2 is suggestive of an α-helical configuration, in which helices of each monomer wind around each other to form a relatively stable, fibrous coiled-coil oligomer. Support for this configuration is evident from electron microscopic images of the S oligomer, which reveal an elongated spike protruding 20 nm from the virion envelope (37). Whether this structural motif is important for virus binding and/or fusion function has not been determined.

Exploration of structure-function relationships in the coronavirus S glycoprotein has relied in part on studies of virus variants. Coronavirus populations, like those of all RNA-containing viruses (35), exhibit considerable genetic heterogeneity, and a variety of variant coronaviruses have been isolated under appropriate selective conditions (2, 14, 36). Selective forces resulting from growth in different cell

types often cause detectable variation of the S glycoprotein, presumably because this molecule plays a key role in host cell recognition. This is readily evident from studies with the coronavirus mouse hepatitis virus type 4 (MHV4, strain JHM). This virus was originally propagated in mice (1). When shifted to long-term growth in tissue culture, selective amplification of variants with both antigenic alterations in S and reduced S-specific fusogenic activity was observed (2, 14, 16). However, complete elimination of neutral pH fusion has never been described.

Here we report that persistent infection of a neural cell line with MHV4 results in the selective amplification of variants that have lost the ability to fuse cells at neutral and basic pH. They are entirely dependent on acid pH to fuse cell membranes. These variants are strongly inhibited by endosomotropic weak bases and thus cannot infect cells without prior internalization into acidic endosomes. We have pinpointed the genetic basis for this loss of neutral pH fusion to as few as three missense mutations, all of which are located in the heptad repeat domain of S2. We conclude that the heptad repeat domains of S2 play a key role in providing a fusion-active conformation and that closely related coronaviruses can exhibit differences in fusion characteristics normally seen only between viruses from entirely different families.

MATERIALS AND METHODS

Cells. Murine cells used for propogation of MHV4 and its variants included DBT (astrocytoma [17]), Sac- (Moloney sarcoma [44]), and OBL21A (retrovirus-transformed neuronal cells derived from the olfactory bulb [28]). HeLa (human carcinoma) cells were used for expression studies. Murine cells were grown as monolayer cultures at 37°C in Dulbecco's modified Eagle's medium (DMEM) supplemented with either 8% calf serum (DBT and Sac-) or 10% fetal calf serum (OBL21A). HeLa cells were grown in minimal essential medium containing 8% calf serum.

Virus and variants. Wild-type MHV4 was propogated in Sac- cells and titers were determined on DBT cell monolayers as described previously (14). To obtain variants of MHV4, persistent infections of various cell lines were established by inoculation with plaque-purified wild-type MHV4 at 0.1 PFU/cell. When persistently infected cells became confluent, supernatant medium from the culture was collected and stored at −70°C. Cells were then passaged by 10-fold dilution into fresh medium. Variant viruses present in the stored supernatants were subjected to three cycles of plaque purification on DBT cells, and virus from final well-isolated plaques was amplified in either Sac- or OBL21A cells, as indicated. When necessary for high-multiplicity infections, stocks of greater than 5×10^6 PFU/ml were prepared by pelleting amplified virus suspensions (25 ml) through sucrose cushions (12 ml, consisting of 4 ml each of 10, 20, and 30% [wt/wt] sucrose in 0.05 M Na-MES [sodium morpholineethanesulfonic acid, pH 6.5]–0.1 M NaCl–0.001 M EDTA). Centrifugation was done at 5°C in a Beckman Spinco SW28 rotor for 4 h at 25,000 rpm.

Variant stocks described in this report are designated as olfactory bulb line variants (OBLV) and are distinguished by their isolation date (days postinfection), e.g., variant OBLV60 was isolated at 60 days postinfection.

Cell fusion assays. Cells were grown in 48-well cluster plates (Corning) to a density of approximately 10^5 cells per cm^2, and then virus was adsorbed (5 PFU/cell) for 1 h at 37°C. The inoculum was removed and replaced with fresh

medium. After 5 h at 37°C, supernatants were removed and replaced with medium (DMEM without $NaHCO_3$ and with 5% calf serum and 20 mM buffer) adjusted to pHs from 5.0 to 8.5. The buffers used were MES (pH 5.0, 5.5, and 6.0), PIPES [piperazine-N,N'-bis(2-ethanesulfonic acid), pH 6.5 and 7.0], HEPES (N-2-hydroxyethylpiperazine-N'-2-ethanesulfonic acid, pH 7.5), and BICINE [N,N-bis(2-hydroxyethyl)glycine, pH 8.0 and 8.5]. After 3 h at 37°C without CO_2, the cells were photographed by phase contrast microscopy. Photos averaging 100 nuclei per exposure were used to quantitate the number of nuclei per cell. Data were tabulated in terms of the fusion index [1 − (cells/nuclei)].

Measurement of virus-specific RNA synthesis. RNA synthesis in virus-infected DBT cells was monitored as described previously (14). Briefly, cells were incubated with dactinomycin (5 μg/ml for 30 min) and then with dactinomycin plus [5,6-^{3}H]uridine (20 μCi/ml for 1 h). Immediately thereafter, lysates were prepared with TNE (0.01 M Tris-HCl [pH 7.0], 0.1 M NaCl, 0.001 M EDTA) containing 1% Nonidet P-40 and spotted onto Whatman GF/C filters. Radioactivity remaining on the filters after successive washes with 20% trichloroacetic acid, 95% ethanol, and diethyl ether was measured by liquid scintillation spectroscopy.

Synthesis and cloning of cDNA. Cytoplasmic RNA was harvested from infected Sac- cells at 16 h postinfection, purified by phenol-chloroform extraction (14), and then fractionated by oligo(dT)-cellulose chromatography (29). The polyadenylated fractions were used as templates in cDNA syntheses, which were performed by the method of Gubler and Hoffman (15). Reverse transcriptase, RNase H, DNA polymerase I, and T4 DNA polymerase were purchased from Amersham. To prime first-strand synthesis, two synthetic oligonucleotides were used separately: oligo 1 (5'-TCTGTCTTTCCAGGAGAGGC-3'), complementary to sequences found 8 to 28 nucleotides downstream of the 4,131-nucleotide S open reading frame, and oligo 2 (5'-CTACGCATAGTCCAGCACCC-3'), complementary to nucleotides 2259 to 2278 of the S gene. Following second-strand replacement synthesis, the double-stranded cDNA was size-fractionated on Sephacryl S-400 spin columns (Pharmacia Corporation) and SalI linkers (New England BioLabs) were ligated to DNAs by using T4 DNA ligase (Promega Corporation). Transcription vector pGEM4Z (Promega) was cut with SalI (Promega), digested with calf intestinal phosphatase (Boeringer Corporation), and then ligated with cDNAs. Competent cells (Epicurian coli XL-1 blue; Stratagene Corporation) were transformed, and clones were screened by colony hybridization with ^{32}P-end-labeled S-specific synthetic oligonucleotides 2 and 3 (5'-CTAAAAT CACCAATATACCC-3', complementary to S nucleotides 40 to 59) by standard methods (29). Positive colonies were amplified and plasmids were purified by anion-exchange chromatography with commercial columns (Qiagen, Inc.).

Full-length cDNAs representing wild-type and OBLV60 S genes were each prepared from partial clones. This was accomplished by excision of S1-encoding HindIII-ApaI fragments and subsequent religation into HindIII-ApaI-digested plasmids encoding S2 sequences (see Fig. 4). The plasmids were designated pS-wt and pS-OBL60, respectively.

Construction of hybrid S genes. Plasmids pS-wt and pS-OBL60 each contain unique restriction sites for HindIII, ClaI, HpaI, and BamHI (see Fig. 4). DNAs (5 μg) were digested to completion with various pairs of these enzymes (Promega) as indicated in the text. The resulting linear DNA molecules were separated by two cycles of electrophoresis on low-melting-point agarose gels (Seaplaque; FMC Corpo-

ration). After each separation, DNAs were purified from gel slices by heating (65°C for 15 min), followed by phenol (four) and chloroform (one) extractions. Ethanol-precipitated DNAs were then used in ligation reactions to generate the recombinant S genes shown in Table 2. After transformation, amplification, and plasmid DNA purification, nucleotide sequencing was used to confirm the desired exchange of restriction fragments.

Nucleic acid sequencing. Both cDNA and direct RNA sequences were determined by the dideoxy primer extension method (30). The primers used and the RNA sequencing methods have been described in detail elsewhere (25). In brief, total cytoplasmic RNA was harvested from acutely infected Sac- cells by phenol extraction as described previously (14), and 10-μg samples were used as templates in sequencing reactions (25). To sequence double-stranded plasmid DNA, templates (2 μg) were alkali denatured and 20-residue primers (20 ng) were annealed. Extension was done with phage T7 DNA polymerase (Pharmacia) in the presence of [^{35}S]dATPαS (Amersham) by published methods (29). Radiolabeled extension products were processed by separation on polyacrylamide gels as described before (25). A typical primer extension analysis permitted determination of 100 to 150 ribonucleotides or 300 to 400 deoxyribonucleotides.

Expression of S glycoprotein from transcription vectors. Confluent cell monolayers were infected with a recombinant vaccinia virus encoding bacteriophage T7 RNA polymerase (vTF7.3 [13]) at a multiplicity of 2 PFU/cell. After 45 min at 37°C, the inoculum was removed, and cells were rinsed three times with serum-free medium and then incubated with 1 ml of serum-free medium containing 25 μg of lipofectin reagent (Bethesda Research Laboratories) and 5 μg of plasmid DNA. Transfected cells were incubated for 4 h at 37°C before addition of 2 ml of serum-containing medium. Expression of S was confirmed by development of syncytia, by detection of radiolabeled S protein, and by indirect surface immunofluorescence with S-specific antibody.

Radiolabeling, immunoprecipitation, endoglycosidase H digestion, and electrophoresis of S glycoprotein. The procedures for detection of the S glycoprotein by radioimmunoprecipitation have been described previously (14). Briefly, infected-cell monolayers were radiolabeled with Tran[^{35}S]-label (ICN Pharmaceuticals, Irvine, Calif.) at the indicated times after infection and lysed with TNE containing 1% Nonidet P-40 and the protease inhibitors aprotinin (1 trypsin inhibitor U/ml) and phenylmethylsulfonyl fluoride (1 mM). Immunoprecipitation of the S glycoprotein from the resulting cytosol was accomplished with rabbit anti-S serum (a gift of K. Holmes, Uniformed Health Services, Bethesda, Md.) and Pansorbin (Calbiochem Corporation) by the method of Kessler (20). Washed Pansorbin pellets were then resuspended in TE containing 1 mM phenylmethylsulfonyl fluoride. For endoglycosidase H digestions, 20-μl aliquots were incubated for 18 h at 37°C after addition of 2 μl of 0.5 M sodium phosphate (pH 6.5), 1 μl of 2% sodium dodecyl sulfate, and 2 μl of endoglycosidase H (Boeringer Corporation; 1 U/ml). Radiolabeled S proteins were removed from Pansorbin by addition of equal volumes of 2× Laemmli sample solubilizer (21), followed by heating to 100°C for 5 min. Proteins were separated on sodium dodecyl sulfate-polyacrylamide gels (21) and visualized by autoradiography.

Indirect immunofluorescence. Cells grown on cover slips were inoculated with MHV4, OBLV60, or vTF7.3 in conjunction with plasmid DNAs pS-wt or pS-OBL60. Cells were fixed at the indicated times after infection in phosphate-buffered saline (PBS) containing 0.2% paraformaldehyde and then incubated with MHV4 S-specific monoclonal antibody (MAb) 4B11.6 (40). Undiluted hybridoma supernatant was used. The secondary antibody was fluorescein isothiocyanate-conjugated sheep anti-mouse immunoglobulin G (The Binding Site, Inc.) and used at a 1:160 dilution in PBS containing 2% bovine serum albumin. After secondary antibody binding, cells were mounted in 90% glycerol containing PBS (pH 8.6) and 25 mg of 1,4-diazobicyclo-2,2,2-octane (19) per ml and photographed with a Nikon Labphot fluorescence microscope. Cell surface fluorescence was quantitated with an adherent cell analysis system 470 interactive laser cytometer (Meridian Instruments, Inc., Okemos, Mich.). This system provided quantitation in terms of average fluorescence per pixel.

RESULTS

Isolation of variants from murine cell lines persistently infected with MHV4. With the goal of isolating novel variants containing alterations in the S gene, we established persistent infection of three murine cell lines with plaque-purified MHV4. Many of our results with two of the cell lines, DBT and Sac-, were not significantly different from those obtained in previous studies (2, 16). In brief, we found that MHV4 infection resulted in extensive syncytium formation, with over 95% cell death by 1 day postinfection. Surviving cells eventually repopulated the culture, and by 1 to 2 months (three to five passages) these cells grew at rates similar to uninfected cells. Virus was continuously present in the supernatants of these cultures; titers fluctuated from 10^2 to over 10^4 PFU/ml. The viruses generally exhibited a small- and clear-plaque phenotype, with cell fusion always evident within the developing plaques (data not shown).

Similar establishment of persistent infection in a cell line derived from murine olfactory bulb neurons, OBL21A, reproducibly yielded several novel results. First, the acute cytotoxic phase of infection seen in the DBT and Sac- cells was not observed. Instead, only occasional microscopic (5 to 10 cell) syncytia were noted 1 day after infection. However, at all subsequent times postinfection, uninfected and infected cultures appeared identical by microscopic examination. The growth rate of the infected cultures was also indistinguishable from that of uninfected control cultures. Second, the titer of virus in the supernatant did not fluctuate but rose continuously, from 6×10^1 PFU/ml at 1 day postinfection to over 10^6 PFU/ml by 45 days postinfection. The percentage of infected cells, as judged by indirect immunofluorescence, also rose steadily from less than 1% after 1 day to over 50% by 45 days (data not shown). After 45 days, titers and infected-cell levels remained high past 160 days. Third, the population of viruses present in supernatants of infected OBL21A cells exhibited alterations in plaque morphology (Fig. 1). Initially the virus produced small plaques. Large-plaque variants predominated between 14 and 45 days postinfection, but the viruses shed at 60 and 80 days generated small, cloudy plaques. Upon microscopic examination, no cell fusion was evident within these cloudy plaques.

Viruses present in supernatants of infected OBL21A cells on the days indicated in Fig. 1 were plaque purified three times on DBT cells and then amplified for 18 h in either Sac- or OBL21A cells to obtain olfactory bulb line variant (OBLV) stocks. We found that the syncytium-negative phenotype of the 60- and 80-day variants was retained throughout plaque purification and amplification and was maintained
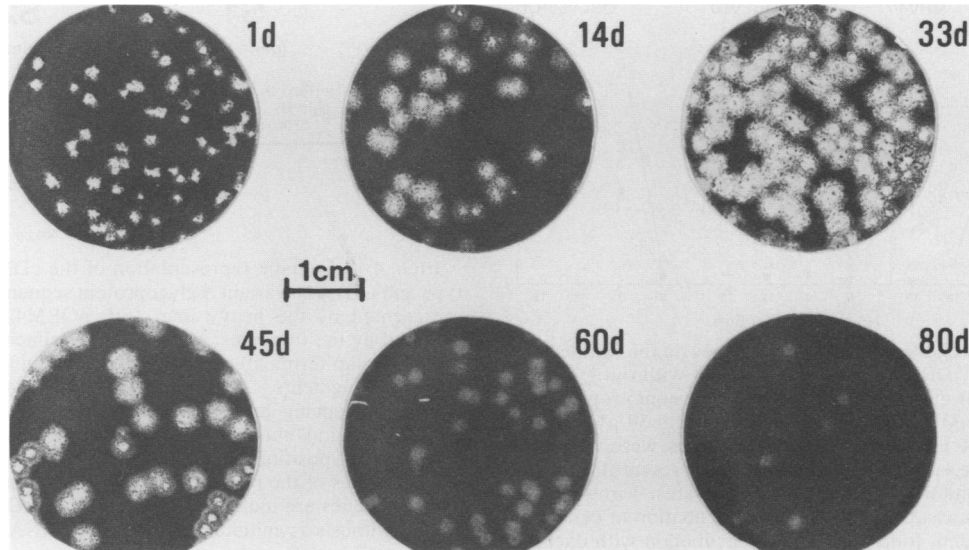
FIG. 1. Plaque morphology of virus variants shed from OBL21A cells persistently infected with MHV4. Variants were collected from cell-free supernatants on the indicated days after establishment of infection and plated on DBT cells for plaque development. After 3 days, cells were fixed and stained for plaque visualization.

upon passage in OBL21A cells. However, continual passage of the 60-day variant (OBLV60) in the Sac- cell line resulted in selection of revertants with restored fusion function. After five successive 18-h growth periods in Sac- cells, initiated each time at 0.1 PFU/cell, 1.5% of the output virus produced syncytia on DBT indicator cells. This reversion to fusion competence was also observed when OBLV60 was used to initiate a persistently infected Sac- cell line. Revertants represented 1% of the virus in supernatants after 14 days and rose to 80% by 21 days postinfection.

Acid pH requirement for fusion function of OBLV60. The loss and restoration of MHV4 fusion function were observed in cultures grown in neutral pH-buffered medium. To determine whether these changes represented a shift in the pH optimum for fusion, we infected confluent DBT and Sac- cell monolayers with wild-type MHV4, OBLV60, or a plaque-purified OBLV60 revertant, OBLV60 R.1. After 6 h, small syncytia occupying about 10% of the monolayers were evident in MHV4-infected cultures. No syncytia were seen in the other cultures. At this time the medium was removed and replaced with medium buffered at pHs from 5.0 to 8.5. In the OBLV60-infected cultures, syncytia developed only at acid pH, with 60% cell fusion after 3 h at pH 5.5 in DBT cells, and similar polykaryon formation at pH 6.0 in Sac-cells (Fig. 2). In contrast, syncytia developed regardless of pH in both the MHV4 and OBLV60 R.1 infections. This extensive fusion at all pHs tested was somewhat different from that seen by Sturman et al. (39) in cultures infected with a related MHV strain, A59. Acid pH was found to inhibit MHV A59 fusion, suggesting that pH thresholds for fusion vary between strains.

Viruses requiring an acidic environment for fusion do not fuse with the plasma membrane but rather are internalized as intact virions into endocytic vesicles. Membrane fusion and release of nucleocapsid into the cytosol do not occur until the virions reach acidic endosomes. Thus, the establishment of infection by these acid-dependent viruses is effectively blocked by weak bases which raise endosomal pH (22).

We tested the effect of two commonly used endosomotro-

pic weak bases, NH_4Cl and chloroquine, on the establishment of infection by wild-type MHV4, OBLV60, and OBLV60 R.1. To monitor the infection cycle, we measured the rate of virus-specific RNA synthesis by quantitation of [^{3}H]uridine incorporation into acid-insoluble RNA in the presence of dactinomycin, a cellular transcription inhibitor that does not inhibit MHV RNA synthesis (26). Incorporation levels observed during a series of 1-h pulses revealed that all viruses tested produced a wave of viral RNA synthesis which peaked at 9 to 12 h postinfection (Fig. 3). In DBT cells treated continuously with either chloroquine or
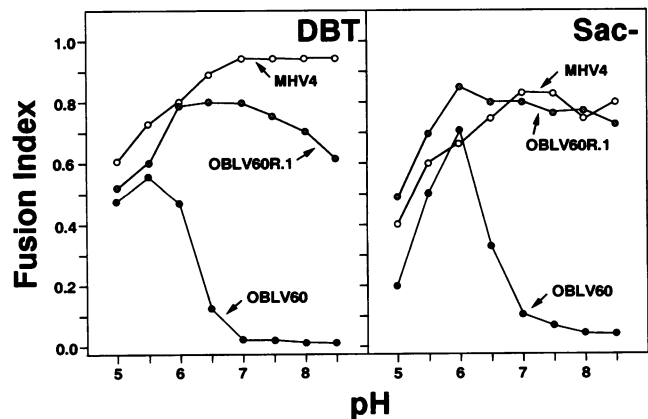

FIG. 2. Effect of medium pH on the development of virus-induced syncytium formation in DBT and Sac- cells. The indicated viruses were used at 5 PFU/cell to infect confluent cell monolayers. After 6 h of infection, the medium (pH 7.1) was removed and replaced with medium buffered to the indicated pH. After an additional 3-h incubation at 37°C without CO_2, the cells were photographed by phase contrast microscopy. Cells and nuclei were counted in representative fields (>100 nuclei per field), and the fusion indices [1 − (cells/nuclei)] were calculated. Fusion indices for uninfected control cultures remained below 0.2 regardless of the pH.
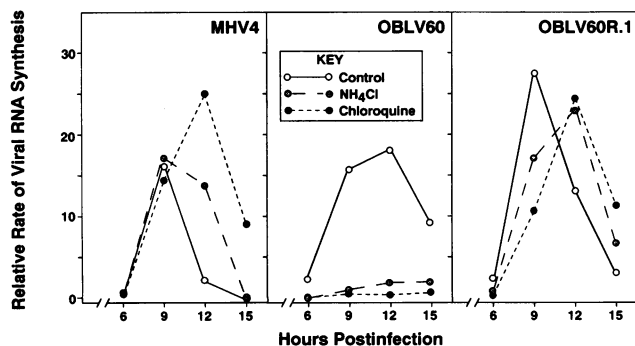
FIG. 3. Effect of endosomotropic weak bases on the synthesis of virus-specific RNA. DBT cells were inoculated with the indicated viruses (5 PFU/cell) and incubated without endosomotropic bases (control), with 20 mM ammonium chloride, or with 50 μM chloroquine present in the growth medium. Weak bases were incubated with cells 1 h before virus inoculation and were present throughout inoculation and monitoring of RNA synthesis rates. Virus-specific RNA synthesis was assayed after a 30-min incubation of cells with dactinomycin (5 μg/ml) followed by a 1-h incubation with dactinomycin plus [5,6-^{3}H]uridine (20 μCi/ml). Data points represent the acid-insoluble radioactivity present in aliquots collected at the end of each labeling period (kcpm of [^{3}H]uridine per 10^5 cells). Radiolabel incorporation levels in mock-infected cells (average, 845 ± 145 cpm per 10^5 cells) were subtracted from each data point.

NH_4Cl beginning at 1 h before infection, OBLV60-specific RNA synthesis was greatly diminished. Chloroquine effectively eliminated viral RNA synthesis, and NH_4Cl reduced RNA synthesis more than 50-fold. In wild-type MHV4- and OBLV60 R.1-infected cultures, neither endosomotropic base prevented the wave of viral RNA synthesis. The bases did, however, delay the onset of OBLV60 R.1 RNA synthesis by 2 to 3 h.

These results were reinforced by our additional finding that continuous chloroquine or NH_4Cl treatment had essentially no inhibitory effect on the production of infectious MHV4 or OBLV60 R.1 in a 16-h growth period. However, the yields of OBLV60 were reduced 50- and 2,500-fold in the presence of NH_4Cl and chloroquine, respectively (Table 1). These two weak bases were most effective in reducing OBLV60 yields when added before inoculation, indicating that they act on early infection events and have little if any directly toxic effect on progeny virus.

Finally, the effects of NH_4Cl and chloroquine on MHV4 and OBLV60 infection were tested in a Sac- cell culture. The

TABLE 1. Effect of chloroquine and NH_4Cl on yield of infectious virus progeny from DBT cells[a]

Treatment	Yield (10^3 PFU/ml) at 16 h postinfection		
	MHV4	OBLV60	OBLV60 R.1
None	0.41	21.0	2.2
Chloroquine			
1 h preinfection	0.65	0.008	1.8
4 h postinfection	0.66	2.4	1.4
NH_4Cl			
1 h preinfection	0.38	0.42	11.0
4 h postinfection	0.15	3.7	8.8

[a] Chloroquine (50 μM) or NH_4Cl (20 mM) was present in the culture medium beginning at the indicated times and maintained thereafter until virus harvest. Progeny virus titers were determined by plaque assay on DBT indicator cells.
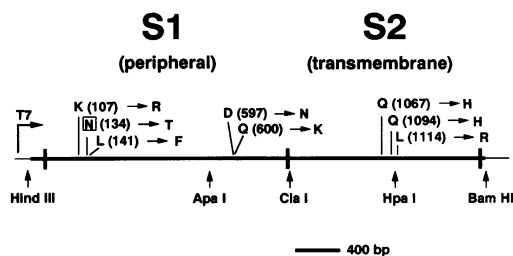

FIG. 4. Schematic representation of the cDNAs encoding wild-type and OBLV60 variant S glycoprotein sequences. The S cDNA is represented by the heavy line, with pGEM4Z vector sequences depicted by the thin lines. Vertical lines delineate segments encoding S1 (amino-terminal) and S2 (carboxy-terminal) posttranslational cleavage fragments. All eight missense mutations identified by cDNA sequencing are shown as wild-type MHV4 → OBLV60 changes. Codon numbers are shown in parentheses. The boxed asparagine at position 134 is potentially glycosylated. Approximate cleavage sites of the restriction enzymes used in the preparation of hybrid S genes are indicated underneath the cDNA representation. RNA synthesis is initiated by phage T7 RNA polymerase at the position of the leftmost arrow.

results (not shown) revealed similar specific inhibition of OBLV60, confirming that use of the endosomal route of entry by OBLV60 is not restricted to the DBT cell line.

cDNA cloning and sequencing of wild-type and OBLV60 S genes. Our results showing acid pH-dependent fusion and inhibition by endosomotropic weak bases indicated that OBLV60, unlike the parental wild-type MHV4, was dependent on the acidic endosomal route of entry into susceptible host cells. Given that, we set out to determine the genetic basis for this difference by cloning, sequencing, and expressing the genes encoding the S glycoprotein of each virus.

DNA copies of the viral S genes were prepared by reverse transcription of polyadenylated RNA collected from infected Sac- cells. Two synthetic oligonucleotide primers complementary to the reported sequence of S (25) were used to initiate S1 and S2 cDNA synthesis. The S2 primer initiated synthesis immediately downstream from the 4,131-nucleotide S open reading frame; the S1 primer annealed near the middle of the S gene. Double-stranded cDNAs were ligated into the in vitro transcription vector pGEM4Z between the T7 and SP6 RNA polymerase promoters and cloned. We initially selected plasmids containing cDNAs greater than 2 kb in length by oligonucleotide colony hybridization. Using primers hybridizing to T7 and SP6 promoter regions, we next determined the sequences of selected cDNA termini by primer extension (30). S1 clones containing MHV4 5' leader sequences (31) and the S initiation codon adjacent to the T7 promoter were selected. Full-length cDNA copies of S were then prepared by excision of inserts from the S1 clones (HindIII-ApaI; Fig. 4), followed by ligation into the large ApaI-HindIII fragments derived from S2 clones. The resulting plasmids were designated pS-wt and pS-OBL60.

Sequencing revealed that both the S-encoding inserts contained 60 nucleotides of MHV4 5' leader sequence (31), the 4,131-nucleotide S open reading frame (25), and 28 nucleotides representing residues immediately 3' to the S gene. The wild-type cDNA (pS-wt) was found to be a faithful representative of the viral S gene; the cDNA sequence differed from direct RNA sequence results (25) in only one position. This was a silent mutation at nucleotide 3990 (C in RNA, T in cDNA clone). Relative to this wild-type clone, the OBLV60 S cDNA (pS-OBL60) differed in a number of
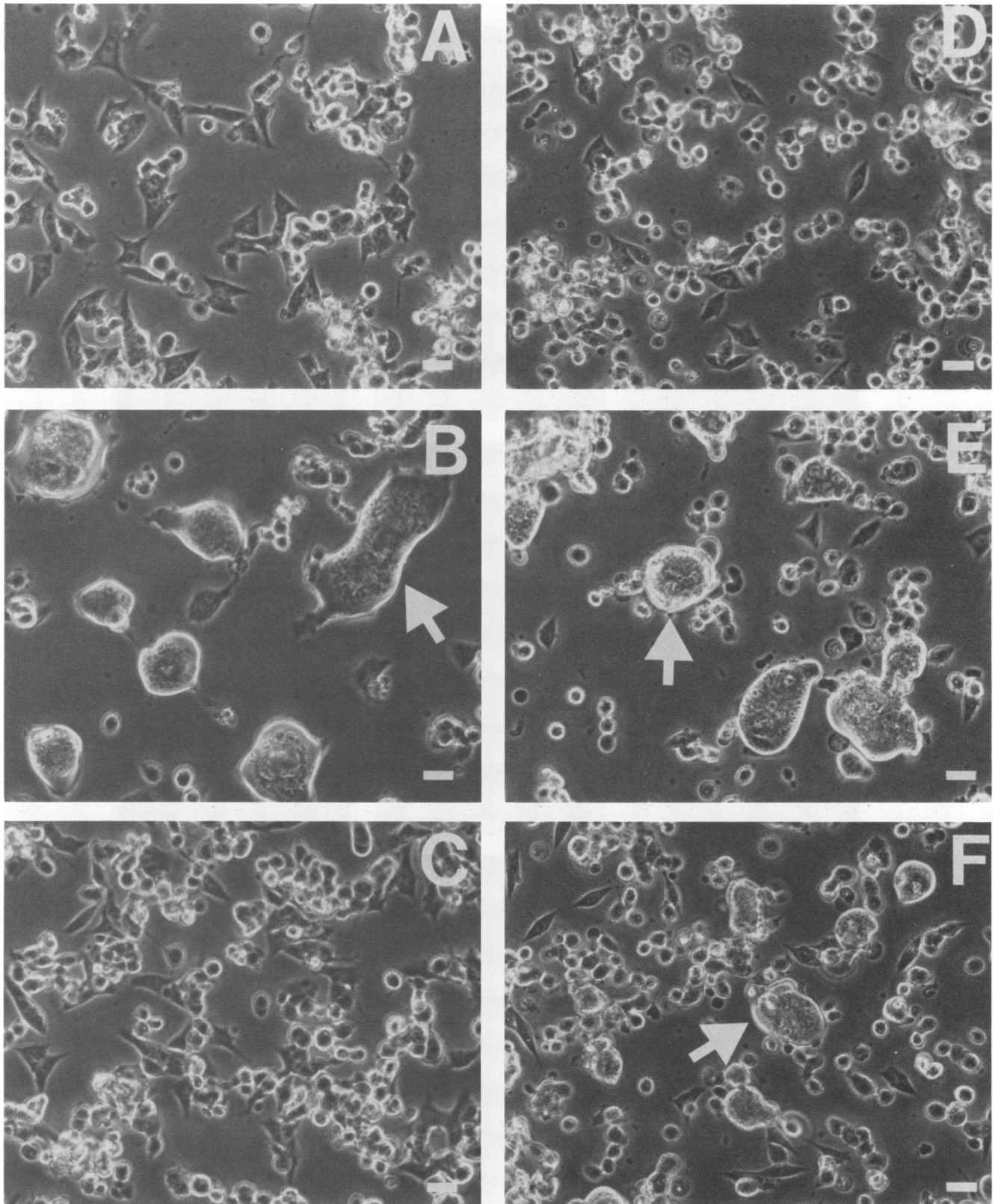
FIG. 5. Demonstration of fusion function of wild-type and OBLV60 S glycoproteins expressed from cDNA. Sac- cells were infected with vTF7.3 and then transfected with control plasmid pS-OBL60-I, which contained an inverse orientation of the S gene (A and D), pS-wt (B and E), or pS-OBL60 (C and F). At 6 h posttransfection, the medium above the cultures depicted in panels D through F was removed and replaced with pH 6.0-buffered medium. After an additional 6-h incubation at 37°C, all cell monolayers were photographed. Arrows point to typical syncytia. Bars, 50 μm.
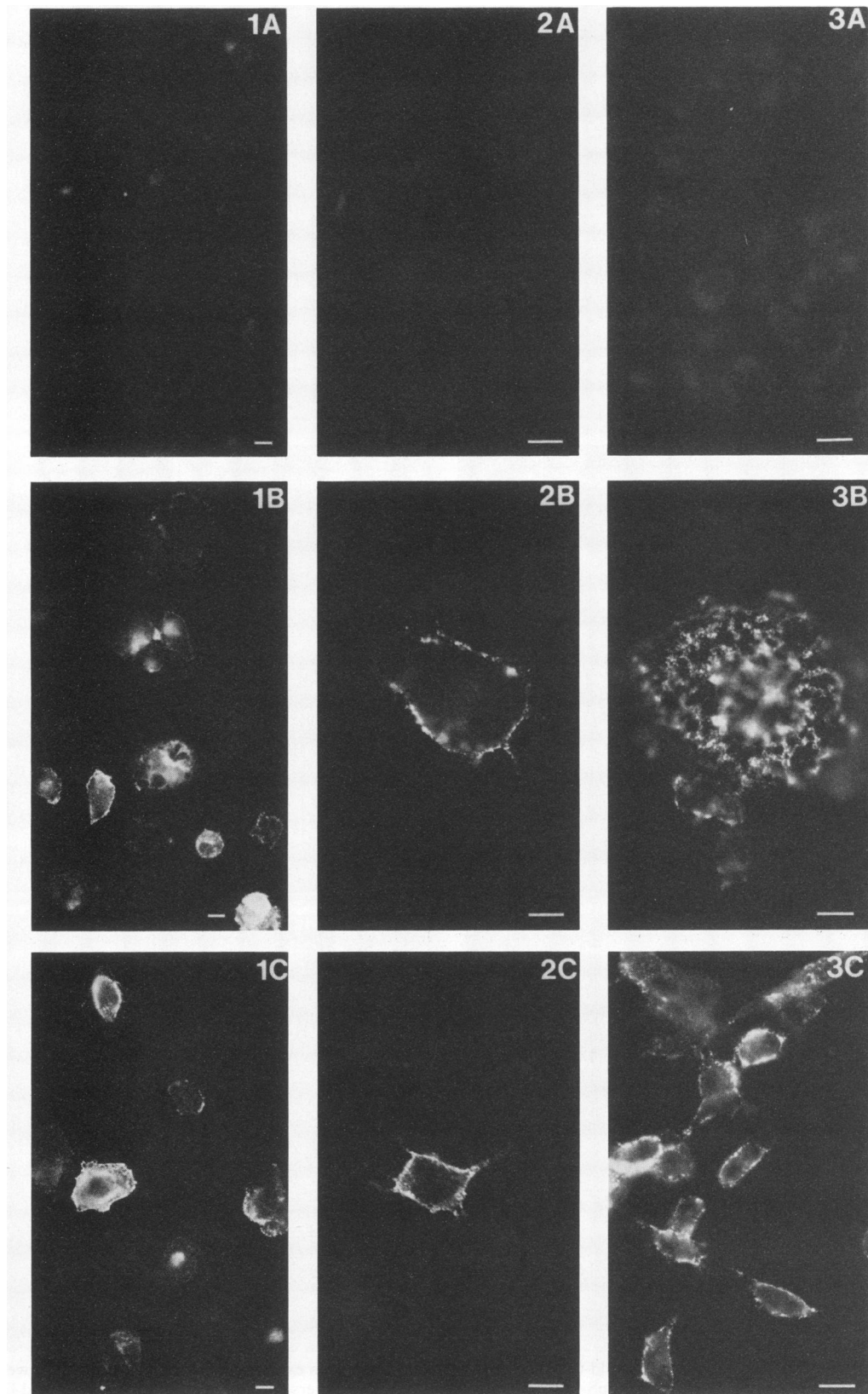
positions. A single silent mutation was present in the leader sequence (wild-type C to A at position −11). More important was the finding of eight mutations in the OBLV60 sequence that created eight amino acid alterations (Fig. 4). These eight mutations fell into three distinct clusters, two in the S1 domain and one in S2. Only two of the eight amino acid changes could be considered conservative (K to R at position 107 and L to F at position 141).

Expression of wild-type and OBLV60 S glycoproteins from cDNA clones. S glycoproteins were expressed directly from pS-wt and pS-OBL60 by lipofectin-mediated transfection of DNAs (11) into cells infected 1 h earlier with the vaccinia virus recombinant vTF7.3 (13). vTF7.3 encodes phage T7 RNA polymerase, which is functional in eukaryotic cytosol. This permits expression of RNA and protein from plasmid DNA located downstream from the phage T7 promoter (Fig. 4).

With this system, the expression of pS-wt and pS-OBL60 was monitored by three different methods. First, expression was detected by microscopic examination of multinucleated syncytia in infected Sac- cells. Sac- cells rather than DBT were chosen for detection of fusion because they were more resistant to the cytopathic effects of vaccinia virus which developed late (>10 h) after infection. In pS-wt-transfected cultures, multinucleated cells began to appear under normal (pH 7.1) culture conditions by 4 h posttransfection. By 12 h posttransfection, cultures were largely fused, with each syncytium containing hundreds of nuclei (Fig. 5B). In contrast, no fusion was observed in parallel cultures transfected with a control pS-OBL60-I, which contained the S cDNA in inverse orientation, or with pS-OBL60 (Fig. 5A and C). Fusion of pS-OBL60-transfected Sac- cells into small polykaryons required a 6-h exposure to pH 6.0-buffered medium (Fig. 5F). This fusion was specific to OBLV60 S expression and not to vaccinia virus infection, since control pS-OBL60-I-transfected cells failed to fuse into characteristic polykaryons upon exposure to pH 6.0 (Fig. 5D).

Second, expression of pS-wt and pS-OBL60 was monitored by indirect cell surface immunofluorescence (Fig. 6). These experiments were done with an MAb (4B11.6) previously shown to react with the wild-type MHV4 S protein (40). Our results demonstrated surface expression of wild-type as well as OBLV60 S in HeLa (human) cells (Fig. 6, panels 1A to 1C) and DBT (mouse) cells (panels 2A to 2C). This cell surface fluorescence was quantitated by scanning more than 200 pS-wt- and pS-OBL60-transfected HeLa cells by interactive laser cytometry. The average surface fluorescence values for cells from these two transfected cultures differed by less than 2% (data not shown). As a control, expression of wild-type and OBLV60 S was assayed on the surface of DBT cells infected with authentic virus (panels 3A to 3C). As expected, polykaryons were observed only in the wild-type virus-infected cells, even though both glycoproteins were found on the cell surface in abundance. Thus, the failure of the OBLV60 S glycoprotein to fuse susceptible cells at neutral pH was not due to a lack of cell surface expression.
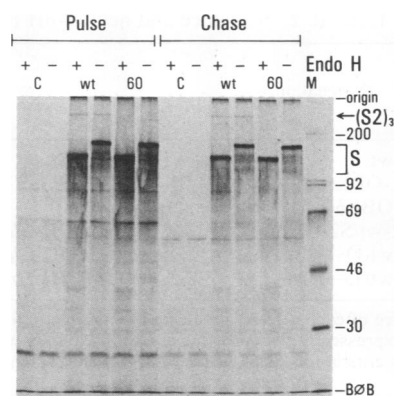

FIG. 7. Relative endoglycosidase H sensitivity of S glycoproteins expressed from cDNA clones. vTF7.3-infected HeLa cells were transfected with control plasmid pS-OBL60-I containing the inverse orientation of S (lanes C), with pS-wt (lanes wt), or with pS-OBL60 (lanes 60). Cultures were then radiolabeled from 4 to 6 h posttransfection.with Tran[^{35}S]-label (200 μCi/ml), and S molecules were immunoprecipitated from selected cultures (pulse). Identical cultures were allowed to continue incubation for 6 h at 37°C in medium containing excess methionine (2 mM) and cysteine (4 mM) prior to immunoprecipitation (chase). Aliquots representing the S proteins collected from 2 × 10⁵ cells were then mock digested (lanes −) or digested with endoglycosidase H (Endo H) (lanes +) prior to electrophoretic separation and visualization by autoradiography. The origin, bromphenol blue (BØB), and molecular mass marker positions (in kilodaltons) are indicated at the right (lane M).

Finally, to determine the relative efficiency of synthesis and transport of the two S glycoproteins, we performed pulse-chase analyses. The autoradiogram in Fig. 7 represents [^{35}S]methionine-labeled S molecules synthesized in HeLa cells from 4 to 6 h after DNA transfection. Both wild-type and OBLV60 S proteins were produced in equivalent amounts, primarily as 180-kDa forms. The relative extent of transport of the two glycoproteins through the Golgi was examined by endoglycosidase H digestion. Glycoproteins acquire resistance to carbohydrate removal by endoglycosidase H only after the processing events associated with transport from the endoplasmic reticulum to the medial Golgi (10). We found that endoglycosidase H treatment of the two glycoproteins, either immediately after the 2-h labeling period or following a 6-h chase, resulted in carbohydrate removal and concomitant generation of a 150-kDa protein (Fig. 7). Only a small proportion of each radiolabeled population possessed endoglycosidase H resistance; this population migrated at 90 to 120 kDa and may represent S1 and S2 processing intermediates. An endoglycosidase H-resistant band designated (S2)₃ in Fig. 7 was also observed between the origin and the 200-kDa marker in pS-wt-transfected cultures; this species has previously been shown to represent an oligomeric form of S2, probably a trimer, that is not disrupted by denaturing gel electrophore-

---

FIG. 6. Indirect cell surface immunofluorescence detection of wild-type and OBLV60 S molecules. HeLa cells (panels 1) or DBT cells (panels 2) were infected with vaccinia virus recombinant vTF7.3 and then transfected with control plasmid pS-OBL60-I, which contained an inverse orientation of the S gene (panels A), pS-wt (panels B), or pS-OBL60 (panels C). At 8 h posttransfection, cells were fixed with paraformaldehyde and incubated with S-specific MAb 4B11.6 (40). Bound MAb was detected with fluorescein isothiocyanate-conjugated anti-mouse immunoglobulin G (1:160). Exposure times were the same for all photographs. Panels 3A through 3C: DBT cells were left uninfected (A) or infected with MHV4 (B) or OBLV60 (C), each at 2 PFU/cell. At 10 h postinfection, cell surface S was detected as described above. Bars, 15 μm.

TABLE 2. Sequence and neutral-pH fusion ability of wild-type, OBL60, and wild-type/OBL60 hybrid S genes

cDNA no.	Designation	Sequence[a]	Neutral pH fusion[b]	Critical S2 residues[c] at position:		
				1067	1094	1114
1	pS-wt	Wild type	+	Q	Q	L
2	pS1-OBL60/S2-wt	S1, OBL60 (HindIII-ClaI); S2, wt (ClaI-BamHI)	+	Q	Q	L
3	pS-OBL60	OBL60	−	H	H	R
4	pS1-wt/S2-OBL60	S1, wt (HindIII-ClaI);S2, OBL60 (ClaI-BamHI)	−	H	H	R
5	pS-wt(Q→H, Q→H)	S1, wt (HindIII-ClaI);S2, OBL60 (ClaI-HpaI), wt (HpaI-BamHI)	+	H	H	L
6	pS-wt(L→R)	S1, wt (HindIII-HpaI);S2, OBL60 (HpaI-BamHI)	+	Q	Q	R

[a] The sequence of each cDNA is indicated by the restriction fragments used to prepare full length S genes.

[b] Ability of expressed S glycoproteins to fuse DBT cells was assessed as described in the legend to Fig. 8. Symbols: +, syncytia evident; −, no syncytia.

[c] All residues critical for fusion at neutral pH were present in the S2 mutation cluster.

sis (14). This stable S2 oligomer was not present in material immunoprecipitated from pS-OBL60-transfected cultures.

Determination of critical residues required for neutral pH fusion. Having established that the wild-type and OBLV60 S glycoproteins expressed from cDNA copies induced pH-independent and acid pH-dependent fusion, respectively, we sought to determine which of the eight mutated residues defined by the sequence comparison contributed to the fusion phenotype. This required expression of S glycoproteins containing various combinations of altered amino acids and was accomplished by exchange of restriction fragments between wild-type and OBL60 S cDNAs. The unique restriction sites for HindIII, ClaI, HpaI, and BamHI were used for fragment exchanges (Fig. 4). Expression analysis of the resulting S hybrids was accomplished by direct transfection into vTF7.3-infected DBT cells, as described above. We confirmed that pS-wt encoded neutral-pH fusion-competent S in DBT cells (Table 2). That mutations in the S2 cluster were solely responsible for this neutral-pH fusion property was shown by separate replacement of wild-type S1 and S2 sequences with OBL60 sequences. A cDNA which encoded OBL60 S1 but wild-type S2 did produce fusion upon transfection, but a cDNA which encoded wild-type S1 but OBL60 S2 did not (Table 2 and Fig. 8), indicating that the S1 mutations were unimportant but the S2 residues Q-1067, Q-1094, and L-1114 were critical for neutral-pH fusion.

To determine which of these three S2 residues was most important for neutral-pH fusion, we used the ClaI, HpaI, and BamHI sites to separate the two Q to H mutations from the L to R mutation (Fig. 4). cDNA 5 (Table 2 and Fig. 8), which encoded H residues at 1067 and 1094 but was otherwise wild type in sequence, encoded fusion-competent S. cDNA 6 encoded a single alteration, L to R at position 1114. Expression of this gene also resulted in syncytium formation; however, the extent of fusion at 6 h posttransfection was markedly lower than that seen in parallel pS-wt-transfected cultures (Fig. 8).

Pulse labeling of all vTF7.3-infected and plasmid DNA-transfected cultures with [35S]methionine followed by radioimmunoprecipitation and electrophoresis of S showed that wild-type, OBL60, and all hybrid S constructs expressed a 180-kDa S protein (Fig. 9). The proteins expressed from DNA copies coelectrophoresed with S produced in an authentic virus infection, suggesting normal glycosylation. Figure 9 also shows that those S glycoproteins harboring the OBL60 S2 mutations were relatively underproduced. This was likely due to the failure of these two S glycoproteins to recruit neighboring untransfected cells into syncytia and thus into the manufacture of greater amounts of S. This contention was supported by results showing equivalent amounts of wild-type and OBL60 S in HeLa cells, which are resistant to fusion by wild-type S (see Fig. 7).

Direct RNA sequencing of OBLV60 and OBLV60 revertants. RNAs collected from virus-infected cell extracts were sequenced directly by the primer extension method to determine whether revertants from acid pH-dependent to pH-independent fusion contained mutations within the cluster of alterations identified by recombinant DNA methods. Sequencing was restricted to nucleotides encoding the S2 amino acid residues 1051 to 1136 (Table 3). Direct RNA sequencing confirmed the existence of substitutions at positions 1067, 1094, and 1114 in OBLV60 that were previously identified by sequencing of cDNA copies. In one of our revertants, R.1, R-1114 had reverted back to L. This cluster of residues in R.1 (H-1067; H-1094, and L-1114) was identical to that present in recombinant cDNA 5 (Table 2), which encoded fusion-competent S. This finding supported the importance of L-1114; however, analysis of an additional revertant, R.3, revealed that the back-mutation of this residue is not absolutely required for restoration of pH-independent fusion. R.3 harbored the three mutations present in OBLV60 as well as a fourth change, V to L, at position 1089.

DISCUSSION

We have found that the pH-independent fusion normally induced by the coronavirus MHV4 can be eliminated by continuous growth of the virus in the OBL21A neural cell culture. We have compared the neural cell-selected fusion variant OBLV60 with parental MHV4 to show that the variant exhibits a unique dependence on acid pH exposure for fusion and a consequent strong requirement for endosome-mediated virus entry. In this regard, the OBLV60 derivative of MHV4 is unlike all known coronaviruses. Thus, one novel conclusion drawn from this study is that pH-independent fusion is not a fundamental property of the Coronaviridae. We also compared MHV4 with OBLV60 by cloning, sequencing, and expressing the fusion glycoprotein (spike, or S) gene of each virus. The results obtained indicate that a cluster of two or three amino acid alterations in the S2 cleavage fragment is responsible for the change in the fusion property.

Cell lines can select for loss or restoration of neutral-pH fusion competence. To obtain variant forms of MHV4, we took advantage of the selective pressures exerted by the cell lines OBL21A and Sac-. In the OBL21A cell line, variants capable of neutral-pH fusion are at a disadvantage relative to viruses that fuse only after acidification. This selective pressure is strong enough to result in relatively homogeneous populations of acid pH-dependent viruses after 2
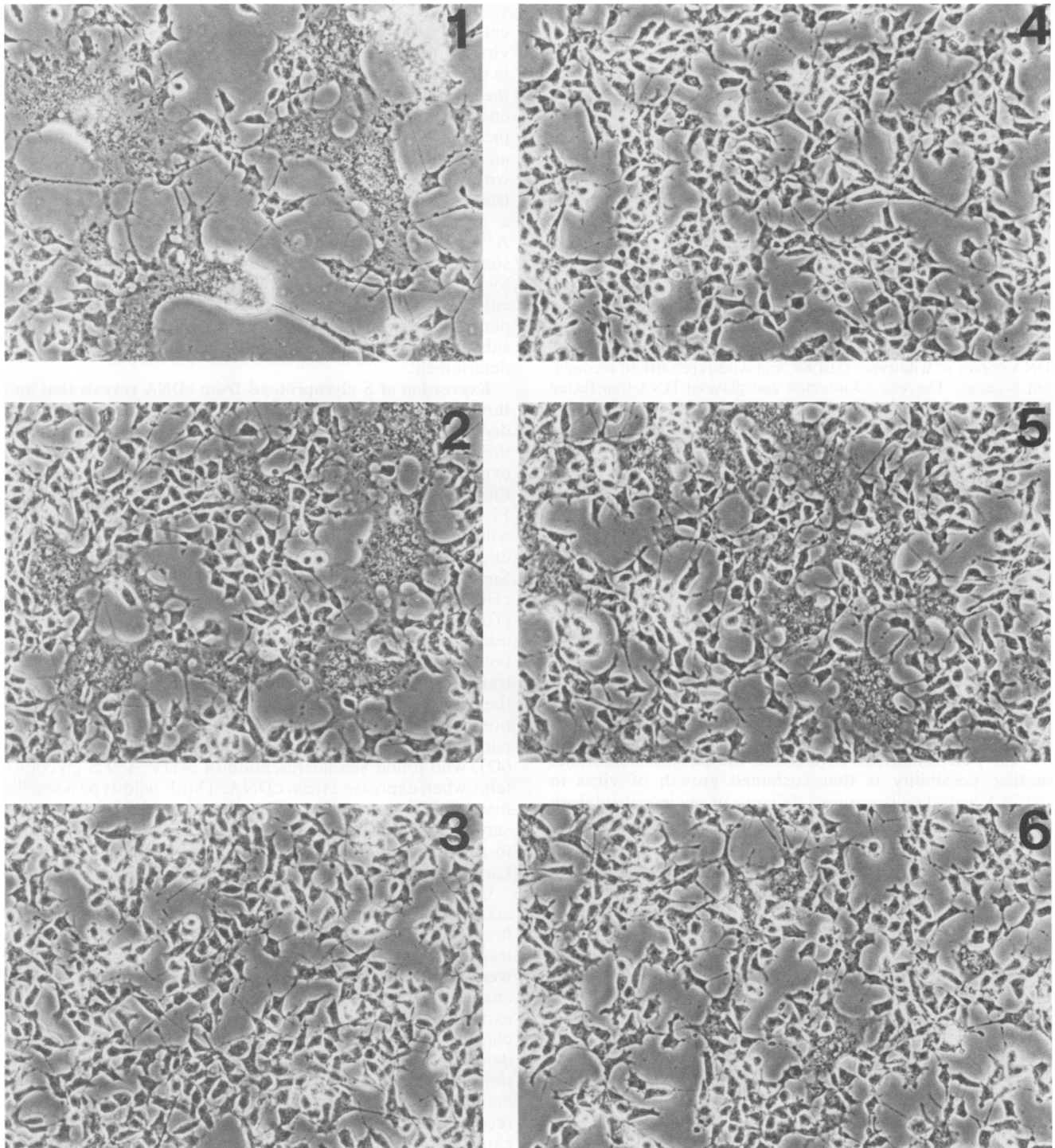
FIG. 8. Fusion capability of MHV S glycoproteins expressed from wild-type, OBL60, and wild-type/OBL60 recombinant cDNA clones. DBT cells (10^5/cm^2) were infected with vaccinia virus-T7 recombinant vTF7.3 at 2 PFU/cell. After 45 min at 37°C, virus was removed, cells were rinsed, and lipofectin-DNA complexes were introduced. After a 6-h incubation at pH 7.1, syncytia were identified by phase contrast microscopy. Numbers on panels indicate transfected DNAs; the sequences of cDNAs 1 through 6 are shown in Table 2.

months of persistent growth. This pattern of virus fitness appears to be reversed in the Sac- cell line, in which acid pH-dependent variants are replaced by neutral-pH-fusing revertants within 3 weeks.

The nature of these selective pressures warrants consideration. For example, it is possible that OBL21A cell membrane composition precludes efficient plasma membrane entry of MHV4 but not entry after endocytosis. In this
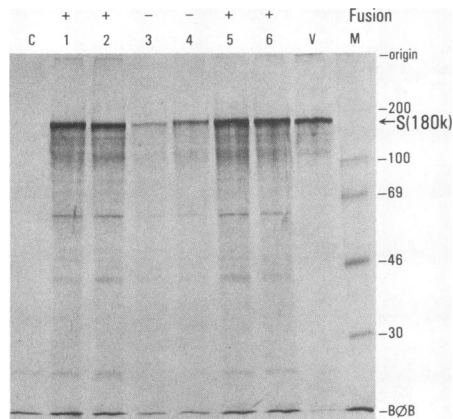
FIG. 9. Demonstration of S glycoprotein synthesis from cloned cDNA copies of wild-type, OBL60, and wild-type/OBL60 recombinant S genes. The vTF7.3-infected and plasmid DNA-transfected DBT cultures depicted in Fig. 8 were radiolabeled from 6 to 8 h after transfection with Tran[^{35}S]-label (0.5 mCi/ml). Cytoplasmic extracts were prepared, and S molecules were immunoprecipitated, electrophoretically separated, and visualized by autoradiography. For electrophoresis, each well was loaded with immunoprecipitates collected from 10^5 cells. Control lane (C), Transfection with pS-wt-I containing S in the inverse orientation. Lanes 1 through 6, Transfection with cDNAs 1 through 6. Virus lane (V), S immunoprecipitated from MHV4-infected DBT cells labeled 8 to 10 h postinfection. Marker lane (M), Molecular mass marker and bromphenol blue (BØB) positions are indicated at the right (in kilodaltons). The neutral pH fusion ability of the cDNA transfectants is shown above lanes 1 to 6 (see Table 2). The S glycoprotein migrated at 180 kDa (180K).

regard, it is notable that membrane cholesterol content (6) and host cell lipid composition (27) have been correlated with the potency of MHV fusion at the plasma membrane. Another possibility is that sustained growth of virus in OBL21A neural cells requires delivery of nucleocapsid deep within the cell body, in a region capable of translating input virion RNA. This is achieved more readily with OBLV60, which fuses only after transport into the endocytic pathway. As for the return to pH-independent fusion competence in Sac- cells, we suspect that these revertant viruses are selectively amplified because they can recruit Sac- cells into massive virus-producing syncytia. Indeed, there is little doubt that cell-to-cell spread of infection via polykaryon formation is advantageous to a virus like MHV, which is known to be extremely labile after it is shed into culture supernatants (39).

MHV4 and OBLV60 exhibit distinct patterns of virus entry. The fact that the presence of NH₄Cl or chloroquine pre-

TABLE 3. Amino acid alterations in the S2 chains of OBLV60 and two OBLV60 revertants[a]

Virus	Fusion[b]	Critical S2 residues at position:			
		1067	1089	1094	1114
Wild type	+	Q	V	Q	L
OBLV60	–	H	V	H	R
OBLV60 R.1	+	H	V	H	L
OBLV60 R.3	+	H	L	H	R

[a] Amino acid alterations were deduced from direct RNA sequences.
[b] Neutral pH fusion function was determined by examination of syncytium formation on infected DBT cells. +, syncytia evident; –, no syncytia.

vented OBLV60 RNA synthesis and PFU production indicated that this virus has an obligate endosomal phase. This virus is not unlike the orthomyxo-, toga-, and rhabdoviruses in this regard (45). All of these viruses require acidification in the endosome to activate fusion. In contrast, blockage of the endosomal route of infection with weak bases did not prevent wild-type MHV4 infection. Thus, at least in DBT and Sac- cells, MHV4 can deliver nucleocapsid via fusion with the plasma membrane. For OBLV60 R.1, endosomotropic weak bases delayed the infection cycle by 2 to 3 h in a manner similar to that previously observed in MHV A59-infected L2 cells treated with NH₄Cl (23). Such a delay suggests that nucleocapsid delivery at the plasma membrane for OBLV60 R.1 is possible but is slow relative to endosomal entry. Whether this is due to relatively slow fusion at the plasma membrane or to ineffective utilization of nucleocapsids delivered just underneath the cell surface remains to be determined.

Expression of S glycoproteins from cDNA reveals that only three amino acid replacements will dramatically alter the pH dependence of fusion. All of the data presented here support the contention that wild-type and OBL60 S glycoproteins expressed from cDNA clones are faithful representatives of the S glycoproteins expressed in authentic virus infections. First, with the exception of a single silent mutation, the wild-type cDNA sequence was identical to that obtained by direct RNA sequencing of the authentic viral S gene (25). Similarly, the three most critical mutations in the OBL60 cDNA sequence were found at the level of the viral RNA (Table 3). Second, both wild-type and OBL60 S glycoproteins were synthesized from cDNA in similar amounts. For both glycoproteins, a small but similar proportion were transported through the exocytic pathway and expressed on the cell surface (Fig. 6 and 7). The finding that both populations of S molecules are largely retained in pre-Golgi compartments was consistent with the results of Vennema et al. (42), who found similar retention of MHV A59 S glycoproteins when expressed from cDNA. Third, wild-type S readily fused MHV-susceptible cells when expressed on the cell surface, but a prolonged exposure to acidic pH was required to activate OBL60 S fusion enough to produce small polykaryons (Fig. 5).

Our sequencing results, therefore, have identified amino acid alterations which act at the level of glycoprotein fusion function and not at the level of glycoprotein synthesis, transport, or surface expression. Eight amino acid changes were identified; glycoproteins containing subsets of these changes were expressed from hybrid S genes. From these expression studies, we found that the five amino acid changes in the S1 cleavage fragment did not play a role in determining the pH threshold for fusion. Thus, the functional significance of the five changes in S1 remains to be determined. Inasmuch as polymorphism among putative receptors for MHV has been reported (3), one attractive explanation is that these S1 alterations enhance virus binding to an OBL21A cell surface receptor. As for the three S2 amino acid changes, we demonstrated that a change from L to R at position 1114 in conjunction with Q to H changes at positions 1067 and 1094 will eliminate neutral-pH fusion. Assessment of the relative importance of each of the Q to H changes to the fusion phenotype will depend upon successful site-specific mutagenesis of codons 1067 and 1094.

How do the amino acid changes in S2 affect fusion function? Figure 10 depicts the three amino acid alterations responsible for changing the pH threshold for fusion in the context of a predicted α-helical configuration. The sequence shown is
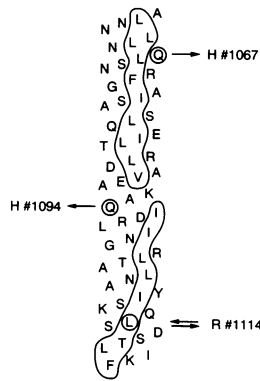
FIG. 10. Helix net depiction of MHV4 S2 amino acid residues 1060 to 1122. The sequence has been identified previously as a heptad repeat domain that is conserved among a wide range of coronavirus spike glycoproteins (7). Hydrophobic faces of the predicted helix are outlined. The two Q to H and the L to R alterations implicated in the loss of neutral-pH fusion are circled. The R-1114 to L change correlated with reversion to neutral-pH fusion competence is indicated by the double arrow.

within the heptad repeat domain common to a number of coronavirus S2 domains (7). Hydrophobic patches (encircled) are readily evident. It is conceivable that these apolar residues act as a coronavirus fusion domain by embedding themselves in the target cell membrane. Exchange of the hydrophobic L-1114 for the large positively charged R would reduce hydrophobicity and impair fusion function. However, this does not explain how a spike carrying R-1114 can be acid pH activated. With respect to acid activation, the two Q to H changes are intriguing. Histidine is unique among the amino acids in its possession of a titratable proton within the physiological pH range ($pK_a = 6.0$). Thus, these H residues could participate in the formation of novel intra- or intermolecular salt bridges upon acid (pH <6) exposure. Repulsive forces between S2 monomers due to acquisition of positive charges might also be important. In this regard, it is notable that protonation of amino acid side chains has been proposed to induce functionally relevant conformational changes in influenza virus hemagglutinin (9, 32). Partial dissociation of the hemagglutinin trimer is one of the proposed changes required for acid-activated orthomyxovirus fusion (32, 46). Similar charge changes or oligomeric dissociations could rearrange the coronavirus spike into a fusion-active conformation.

We anticipate that a range of amino acid alterations correlated with restoration of pH-independent fusion will be found as more OBLV60 revertants are isolated and sequenced. At present, the two revertants that have been partially sequenced support the importance of amino acid residues within the heptad repeat domain. However, the possibility of additional S gene mutations in the OBLV60 revertants remains. Any changes identified by direct RNA sequencing will therefore have to be introduced into and expressed from fully sequenced cDNA clones. This is particularly true for the conservative V to L change identified at position 1089 on OBLV60 R.3. Expression of additional S glycoproteins with altered fusion function will surely increase our knowledge of the structural and functional relationships that exist in the coronavirus spike.

REFERENCES

1. **Bailey, O. T., A. M. Pappenheimer, F. S. Cheever, and J. B. Daniels.** 1949. A murine virus (JHM) causing disseminated encephalomyelitis with extensive destruction of myelin. II. Pathology. J. Exp. Med. **90:**195–212.
2. **Baybutt, H. N., H. Wege, M. J. Carter, and V. ter Meulen.** 1984. Adaptation of coronavirus JHM to persistent infection of murine Sac- cells. J. Gen. Virol. **65:**915–924.
3. **Boyle, J. F., D. G. Weismiller, and K. V. Holmes.** 1987. Genetic resistance to mouse hepatitis virus correlates with absence of virus-binding activity on target tissues. J. Virol. **61:**185–190.
4. **Cavanaugh, D.** 1983. Coronavirus IBV: structural characterization of the spike protein. J. Gen. Virol. **64:**2577–2583.
5. **Cohen, C., and D. A. D. Parry.** 1986. Alpha-helical coiled coils—a widespread motif in proteins. Trends Biochem. Sci. **11:**245–248.
6. **Daya, M., M. Cervin, and R. Anderson.** 1988. Cholesterol enhances mouse hepatitis virus-mediated cell fusion. Virology **163:**276–283.
7. **deGroot, R. J., W. Luytjes, M. C. Horzinek, B. A. M. van der Zeijst, W. J. M. Spaan, and J. A. Lenstra.** 1987. Evidence for a coiled-coil structure in the spike proteins of coronaviruses. J. Mol. Biol. **196:**963–966.
8. **Delmas, B., and H. Laude.** 1990. Assembly of coronavirus spike protein into trimers and its role in epitope expression. J. Virol. **64:**5367–5375.
9. **Doms, R. W., A. Helenius, and J. M. White.** 1985. Membrane fusion activity of the influenza virus hemagglutinin: the low pH induced conformational change. J. Biol. Chem. **260:**2973–2981.
10. **Dunphy, W. G., and J. E. Rothman.** 1985. Compartmental organization of the Golgi stack. Cell **42:**13–21.
11. **Felgner, P. L., T. R. Gadek, M. Holm, R. Roman, H. W. Chan, M. Wenz, J. P. Northrop, G. M. Ringold, and G. A. Daniels.** 1987. Lipofectin: highly efficient, lipid-mediated DNA transfection procedure. Proc. Natl. Acad. Sci. USA **84:**7413–7417.
12. **Frana, M. F., J. N. Behnke, L. S. Sturman, and K. V. Holmes.** 1985. Proteolytic cleavage of the E2 glycoprotein of murine coronavirus: host-dependent differences in proteolytic cleavage and cell fusion. J. Virol. **56:**912–920.
13. **Fuerst, T. R., E. G. Niles, F. W. Studier, and B. Moss.** 1986. Eukaryotic transient-expression system based on recombinant vaccinia virus that synthesizes bacteriophage T7 RNA polymerase. Proc. Natl. Acad. Sci. USA **83:**8122–8126.
14. **Gallagher, T. M., S. E. Parker, and M. J. Buchmeier.** 1990. Neutralization-resistant variants of a neurotropic coronavirus are generated by deletions within the amino-terminal half of the spike glycoprotein. J. Virol. **64:**731–741.
15. **Gubler, U., and B. J. Hoffman.** 1983. A simple and very efficient method for generating cDNA libraries. Gene **25:**263–269.
16. **Hirano, N., N. Goto, S. Makino, and K. Fujiwara.** 1981. Persistent infection with mouse hepatitis virus JHM strain in DBT cell culture, p. 301–308. In V. ter Meulen, S. Siddell, and H. Wege (ed.), Biochemistry and biology of coronaviruses. Plenum Publishing Corp., New York.
17. **Hirano, N., T. Murakami, K. Fujiwara, and M. Matsumoto.** 1978. Utility of mouse cell line DBT for propagation and assay of mouse hepatitis virus. Jpn. J. Exp. Med. **48:**71–75.
18. **Holmes, K. V., J. F. Boyle, R. K. Williams, C. B. Stephensen, S. G. Robbins, E. C. Bauer, C. S. Duchala, M. F. Frana, D. G. Weismiller, S. Compton, J. J. McGowan, and L. S. Sturman.** 1987. Processing of coronavirus proteins and assembly of virions, p. 339–349. In M. A. Brinton and R. R. Rueckert (ed.), Positive-strand RNA viruses. Alan R. Liss, Inc., New York.
19. **Johnson, G. D., R. S. Davidson, K. C. McNamee, G. Russell, D. Goodwin, and E. J. Holborow.** 1982. Fading of immunofluores-

cence during microscopy: a study of the phenomenon and its remedy. J. Immunol. Methods **55**:231–242.

20. **Kessler, S.** 1976. Cell membrane antigen isolation with the staphylococcal protein A-antibody. J. Immunol. **117**:1482–1490.

21. **Laemmli, U. K.** 1970. Cleavage of structural proteins during the assembly of the head of bacteriophage T4. Nature (London) **227**:680–685.

22. **Marsh, M., and A. Helenius.** 1989. Virus entry into animal cells. Adv. Virus Res. **36**:107–151.

23. **Mizzen, L., A. Hilton, S. Cheley, and R. Anderson.** 1985. Attenuation of murine coronavirus infection by ammonium chloride. Virology **142**:378–388.

24. **Niemann, H., B. Boschek, D. Evans, M. Rosing, T. Tamura, and H. D. Klenk.** 1982. Posttranslational glycosylation of coronavirus glycoprotein E1: inhibition by monensin. EMBO J. **1**:1499–1504.

25. **Parker, S. E., T. M. Gallagher, and M. J. Buchmeier.** 1989. Sequence analysis reveals extensive polymorphism and evidence of deletions within the E2 glycoprotein of several strains of murine hepatitis virus. Virology **173**:664–673.

26. **Robb, J. A., and C. W. Bond.** 1989. Coronaviridae, p. 193–247. *In* H. Fraenkel-Conrat and R. R. Wagner (ed.), Comprehensive virology, vol. 14. Plenum Publishing Corp., New York.

27. **Roos, D. S., C. S. Duchala, C. B. Stephensen, K. V. Holmes, and P. W. Choppin.** 1990. Control of virus-induced cell fusion by host cell lipid composition. Virology **175**:345–347.

28. **Ryder, E. F., E. V. Snyder, and C. L. Cepko.** 1990. Establishment and characterization of multipotent neural cell lines using retrovirus vector-mediated oncogene transfer. J. Neurobiol. **21**:356–375.

29. **Sambrook, J., E. F. Fritsch, and T. Maniatis.** 1989. Molecular cloning: a laboratory manual, 2nd ed. Cold Spring Harbor Laboratory, Cold Spring Harbor, N.Y.

30. **Sanger, F., S. Nicklen, and A. R. Coulson.** 1977. DNA sequencing with chain-terminating inhibitors. Proc. Natl. Acad. Sci. USA **74**:5463–5467.

31. **Shieh, C. K., L. H. Soe, S. Makino, M. F. Chang, S. A. Stohlman, and M. M. C. Lai.** 1987. The 5'-end sequence of the murine coronavirus genome: implications for multiple fusion sites in leader-primed transcription. Virology **156**:321–330.

32. **Skehel, J. J., P. M. Bayley, E. B. Brown, S. R. Martin, M. D. Waterfield, J. M. White, I. A. Wilson, and D. C. Wiley.** 1982. Changes in the conformation of influenza virus hemagglutinin at the pH optimum of virus-mediated membrane fusion. Proc. Natl. Acad. Sci. USA **79**:968–972.

33. **Spaan, W., D. Cavanaugh, and M. C. Horzinek.** 1988. Corona-

viruses: structure and genome expression. J. Gen. Virol. **69**: 2939–2952.

34. **Stegmann, T., R. W. Doms, and A. Helenius.** 1989. Protein-mediated membrane fusion. Annu. Rev. Biophys. Biophys. Chem. **18**:187–211.

35. **Steinhauer, D. A., and J. J. Holland.** 1987. Rapid evolution of RNA viruses. Annu. Rev. Microbiol. **41**:409–433.

36. **Stohlman, S., P. Brayton, J. Fleming, L. Weiner, and M. Lai.** 1982. Murine coronaviruses: isolation and characterization of two plaque morphology variants of JHM neurotropic strain. J. Gen. Virol. **63**:265–275.

37. **Sturman, L. S., K. V. Holmes, and J. Behnke.** 1980. Isolation of coronavirus envelope glycoproteins and interaction with the viral nucleocapsid. J. Virol. **33**:449–462.

38. **Sturman, L. S., C. S. Ricard, and K. V. Holmes.** 1985. Proteolytic cleavage of the E2 glycoprotein of murine coronavirus: activation of cell-fusing activity of virions by trypsin and separation of two different 90K cleavage fragments. J. Virol. **56**:904–911.

39. **Sturman, L. S., C. S. Ricard, and K. V. Holmes.** 1990. Conformational change of the coronavirus peplomer glycoprotein at pH 8.0 and 37°C correlates with virus aggregation and virus-induced cell fusion. J. Virol. **64**:3042–3050.

40. **Talbot, P. J., A. A. Salmi, R. L. Knobler, and M. J. Buchmeier.** 1984. Topographical mapping of epitopes on the glycoproteins of murine hepatitis virus-4 (strain JHM): correlation with biological activities. Virology **132**:250–260.

41. **Tooze, S. A., J. Tooze, and G. Warren.** 1988. Site of addition of *N*-acetylgalactosamine to the E1 glycoprotein of mouse hepatitis virus-A59. J. Cell Biol. **106**:1475–1487.

42. **Vennema, H., L. Heijnen, A. Zijderveld, M. C. Horzinek, and W. J. M. Spaan.** 1990. Intracellular transport of recombinant coronavirus spike proteins: implications for virus assembly. J. Virol. **64**:339–346.

43. **Von Heijne, G.** 1984. A new method for predicting signal sequence cleavage sites. Nucleic Acids Res. **14**:4683–4690.

44. **Weiland, M., M. Mussgay, and F. Weiland.** 1978. Nonproducer malignant tumor cells with rescuable sarcoma virus genome isolated from a recurrent Moloney sarcoma. J. Exp. Med. **148**:408–423.

45. **White, J. M.** 1990. Viral and cellular membrane fusion proteins. Annu. Rev. Physiol. **52**:675–97.

46. **White, J. M., and I. A. Wilson.** 1987. Anti-peptide antibodies detect steps in a protein conformational change: low pH activation of the influenza virus hemagglutinin. J. Cell Biol. **105**:2887–2896.